THE ASTROPHYSICAL JOURNAL, 559:187–195, 2001 September 20

SIMULTANEOUS X-RAY AND TeV GAMMA-RAY OBSERVATION OF THE TeV BLAZAR MARKARIAN 421 DURING 2000 FEBRUARY AND MAY

H. KRAWCZYNSKI,[1,2] R. SAMBRUNA,[3] A. KOHNLE,[2] AND P. S. COPPI[1]
AND
F. AHARONIAN,[2] A. AKHPERJANIAN,[4] J. BARRIO,[5,6] K. BERNLÖHR,[2] H. BÖRST,[7] H. BOJAHR,[8] O. BOLZ,[2] J. CONTRERAS,[5] J. CORTINA,[5] S. DENNINGHOFF,[5] V. FONSECA,[6] J. GONZALEZ,[6] N. GÖTTING,[9] G. HEINZELMANN,[9] G. HERMANN,[2] A. HEUSLER,[2] W. HOFMANN,[2] D. HORNS,[2] A. IBARRA,[6] I. JUNG,[2] R. KANKANYAN,[2] M. KESTEL,[5] J. KETTLER,[2] A. KONOPELKO,[2] H. KORNMEYER,[5] D. KRANICH,[5] H. LAMPEITL,[2] E. LORENZ,[5] F. LUCARELLI,[6] N. MAGNUSSEN,[8] O. MANG,[7] H. MEYER,[8] R. MIRZOYAN,[5] A. MORALEJO,[6] L. PADILLA,[9] M. PANTER,[2] R. PLAGA,[6] A. PLYASHESHNIKOV,[2,10] G. PÜHLHOFER,[2] G. RAUTERBERG,[7] A. RÖHRING,[9] W. RHODE,[8] G. ROWELL,[2] V. SAHAKIAN,[4] M. SAMORSKI,[7] M. SCHILLING,[7] F. SCHRÖDER,[8] M. SIEMS,[7] W. STAMM,[7] M. TLUCZYKONT,[9] H. J. VÖLK,[2] C. A. WIEDNER,[2] AND W. WITTEK[5]
(THE HEGRA COLLABORATION)

Received 2001 March 20; accepted 2001 May 18

ABSTRACT

We present the results of simultaneous observations of the TeV blazar Markarian 421 at X-ray and TeV gamma-ray energies with the *Rossi X-Ray Timing Explorer* and the stereoscopic Cerenkov telescope system of the High Energy Gamma-Ray Astronomy (HEGRA) experiment, respectively. The source was monitored from 2000 February 2 to 16 and from 2000 May 3 to 8. In both energy bands several flares with very rapid flux variability were observed. In the X-ray band, the flux increased and decreased with *e*-folding times as short as about 5 hr. The 3–20 keV photon index varied between values of 2.2 and 2.9. For five pointings the data show statistically significant evidence for spectral curvature. The photon index varied substantially on very short timescales: on 2000 February 11 it hardened within 1.6 hr by $\Delta\Gamma = 0.18$, and on February 14 it softened within 1.6 hr by $\Delta\Gamma = 0.2$. The TeV observations of February 7/8 showed statistically significant evidence for substantial TeV flux variability on a 30 minute timescale. The TeV energy spectrum averaged over all the observations of the campaign shows a similar steep slope as in earlier HEGRA observations: $dN/dE = N_0(E/1\ \mathrm{TeV})^{-\Gamma}$ with $N_0 = (25 \pm 1_{\mathrm{stat}}) \times 10^{-12}$ photons cm^{-2} s^{-1} TeV^{-1} and $\Gamma = 2.94 \pm 0.06_{\mathrm{stat}}$. Within statistical errors no evidence for a curvature of the TeV energy spectrum is found. We show the results of modeling the data with a time-dependent homogeneous synchrotron self-Compton model. The X-ray and TeV gamma-ray emission strengths and energy spectra together with the rapid flux variability strongly suggest that the emission volume is approaching the observer with a Doppler factor of 50 or higher. The different flux variability timescales observed at X-rays and TeV gamma rays indicate that a more detailed analysis will require inhomogeneous models with several emission zones.

Subject headings: BL Lacertae objects: individual (Markarian 421) — galaxies: jets — gamma rays: observations

1. INTRODUCTION

Since its early detection as a source of TeV gamma rays (Punch et al. 1992; Petry et al. 1996), the BL Lacertae object Markarian 421 ($z = 0.031$) has been subject to very intensive studies throughout the electromagnetic spectrum. The study of this extreme gamma-ray–loud blazar promises to elucidate the origin of jets of active galactic nuclei (AGNs). Furthermore, the source is a laboratory for performing time-resolved studies of the processes of particle acceleration and cooling. With a luminosity per solid angle of about 10^{44} ergs s^{-1} sr^{-1}, Mrk 421 is clearly a low-luminosity blazar. Nevertheless, the central black hole is estimated to be rather massive; Gorham et al. (2000) estimate a mass of between 1.8×10^8 and $3.6 \times 10^9\ M_\odot$.

Mrk 421 has been studied intensively at X-ray energies. Schubnell (1996) used the pointed X-ray telescopes on board the *Rossi X-Ray Timing Explorer* (*RXTE*) satellite to monitor the source over a time period of 17 days. The 2–10 keV flux varied throughout the campaign by a factor of 10, while the photon index showed values between 2.3 and 3.4. Very detailed observations with integration times of several days were carried through with the *BeppoSAX* instruments during 1997 and 1998 (Guainizzi et al. 1999; Malizzia et al. 2000; Fossati et al. 2000a, 2000b). Photon statistics limited the range in which the spectrum could be determined to between 0.1 and ~15 keV. While single–power-law and

[1] Yale University, P.O. Box 208101, New Haven, CT 06520-8101; krawcz@astro.yale.edu.
[2] Max-Planck-Institut für Kernphysik, Postfach 103980, D-69029 Heidelberg, Germany.
[3] George Mason University, 4400 University Drive, M/S 3F3, Fairfax, VA 22030.
[4] Yerevan Physics Institute, Alikhanian Br. 2, 375036 Yerevan, Armenia.
[5] Max-Planck-Institut für Physik, Föhringer Ring 6, D-80805 München, Germany.
[6] Universidad Complutense, Facultad de Ciencias Físicas, Ciudad Universitaria, E-28040 Madrid, Spain.
[7] Universität Kiel, Institut für Experimentelle und Angewandte Physik, Leibnizstrasse 15-19, D-24118 Kiel, Germany.
[8] Universität Wuppertal, Fachbereich Physik, Gaussstrasse 20, D-42097 Wuppertal, Germany.
[9] Universität Hamburg, II. Institut für Experimentalphysik, Luruper Chaussee 149, D-22761 Hamburg, Germany.
[10] On leave from Altai State University, 66 Dimitrov Street, Barnaul 656099, Russia.

broken power-law fits did not describe the data satisfactorily, a model of the form $F(E) = KE^{\alpha_1}[1 + (E/E_b)^f]^{(\alpha_1 - \alpha_2)/f}$ incorporating continuous curvature resulted in statistically acceptable fits to the data (Fossati et al. 2000b). The spectral energy distribution (SED) was found to peak in the energy range between 0.1 and 1.1 keV or below 0.1 keV outside the energy range covered by the observations. The spectral slope around 5 keV was described by photon indices between 2.5 and 3.2.

At TeV energies, Mrk 421 shows rapid flux variability on timescales down to a fraction of an hour (Gaidos et al. 1996). Within statistical errors the Mrk 421 energy spectra measured so far are consistent with pure power-law spectra. The Whipple collaboration reported 260 GeV–10 TeV photon indices of $2.54 \pm 0.04_{\rm stat} \pm 0.1_{\rm syst}$ and $2.45 \pm 0.1_{\rm stat} \pm 0.1_{\rm syst}$ for two very strong flares measured on 1996 May 7 and 16 with integral fluxes above a threshold energy of 350 GeV of 7.4 and 2.8 crab, respectively (Krennrich et al. 1999). The HEGRA collaboration reported steeper 0.5–5 TeV photon indices during several medium-strong flares during 1997 and 1998 (between 1 and 2 crab above 1 TeV) without statistically significant evidence for a departure from the 1997–1998 mean index of $3.09 \pm 0.07_{\rm stat} \pm 0.1_{\rm syst}$ (Aharonian et al. 1999c).

The broadband flux variability was studied in several intensive observation campaigns and led to the discovery of pronounced TeV gamma-ray/X-ray flux correlations (Buckley et al. 1996; Takahashi et al. 1996). Recently, Takahashi et al. (2000) combined the results of intensive UV and X-ray observations performed with the *Extreme Ultraviolet Explorer*, *BeppoSAX*, and *ASCA* in 1998 April with the TeV light curves measured with the Cerenkov Array at Themis, HEGRA, and Whipple Cerenkov telescopes. The UV/X-ray flux showed "quasi-periodic" oscillations with a period of approximately 0.5 days and seemed to be well correlated with the TeV flux.

After observations in early 2000 February with the HEGRA Cerenkov telescopes and the All-Sky Monitor on board the *RXTE* satellite showed increased TeV gamma-ray and X-ray activity of the source at a flux level comparable to the flux of the Crab Nebula, we asked the *RXTE* Guest Observatory Facility (GOF) to use a fraction of *RXTE* AO5 time, originally intended for monitoring Mrk 501, to observe the more active source Mrk 421.

In this paper we present the results of the coordinated X-ray (*RXTE*) and TeV gamma-ray (HEGRA) observations performed on 2000 February 2–16 and May 3–8. The rest of the paper is structured as follows: In § 2 we describe the X-ray and TeV gamma-ray data samples and data reduction, and in § 3 we present the observational results, i.e., the X-ray and TeV gamma-ray light curves, the flux correlation properties, the search for the shortest timescales of flux and spectral variability, and the X-ray and TeV energy spectra. In § 4 we discuss the observational results in the framework of synchrotron self-Compton (SSC) models.

2. X-RAY AND TeV GAMMA-RAY DATA SETS AND DATA REDUCTION

2.1. *X-Ray Data*

The X-ray analysis described in the following is based on the 3–20 keV data from the Proportional Counter Array (PCA; Jahoda et al. 1996) on board the *RXTE* satellite. We did not use the 15–250 keV data from the High-Energy X-ray Timing experiment (Rothschild et al. 1998) because of poor signal-to-noise ratio. Standard-2 mode PCA data gathered with the top layer of the operational proportional counter units (PCUs) were analyzed. The number of PCUs operational during a pointing varied between 2 and 5. After applying the standard screening criteria, the net exposure in each good time interval ranged from 16 s to 3.15 ks (see Table 2). Spectra and light curves were extracted with FTOOLS v5.0. Background models were generated with the tool *pcabackest*, based on the *RXTE* GOF calibration files for a "faint" source (less than 40 counts s^{-1} PCU^{-1}). Response matrices for the PCA data were created with the script PCARSP v2.43. The spectral analysis was performed with the XSPEC v11.0.1 package. A constant neutral hydrogen column density of 2×10^{20} cm^{-2} was chosen, a value that lies close to the 21 cm line H I result of 1.6×10^{20} cm^{-2} (Dickey & Lockman 1990) and the *BeppoSAX* spectral absorption result of $(1.7–3.8) \times 10^{20}$ cm^{-2} (Fossati et al. 2000b). Since the analysis is restricted to the energy region above 3 keV, the chosen hydrogen column density has only a very minor influence on the estimated model parameters. The majority of measurements were satisfactorily described with single–power-law models; for days with long integration times and high count rates, single–power-law models did not describe the data satisfactorily and we fitted broken power-law models. The quoted uncertainties on the spectral parameters are on the 67% confidence level ($\Delta\chi^2 = 1$) for the parameters of interest.

2.2. *TeV Gamma-Ray Data*

The TeV gamma-ray analysis presented in this paper is based on observations with the HEGRA Cerenkov telescope system (Konopelko et al. 1999) located on the Roque de los Muchachos on the Canary Island of La Palma (latitute N28°.8, longitude W17°.9, 2200 m above sea level). The observations comprise a total of 61 hours of best-quality data. The analysis tools, the procedures of data cleaning and fine-tuning of the Monte Carlo simulations, and the estimate of the systematic errors on the differential gamma-ray energy spectra were discussed in detail by Aharonian et al. (1999a, 1999b). The analysis uses the standard "loose" gamma/hadron separation cuts, which minimize systematic errors on flux and spectral estimates rather than yielding the optimal signal-to-noise ratio. A software requirement of two triggered Cerenkov telescopes within 200 m from the shower axis, each with more than 40 photoelectrons per image and a "distance" parameter of smaller than 1°.7, was used. Additionally, only events with a stereo angle larger than 20° were admitted to the analysis. Integral fluxes for certain energy intervals were obtained by integrating the differential energy spectra over the relevant energy region. By this means, the zenith angle dependence of the effective area has been corrected for, and the results are largely independent of the assumed energy spectrum. For data runs during which the weather or the detector performance caused a cosmic-ray detection rate deviating only slightly, i.e., less than 15%, from the expectation value, the gamma-ray detection rates and spectra were corrected accordingly. Spectra and fluxes above an energy threshold of 500 GeV were derived from the 43 hours of data from zenith angles smaller than 30°. The search for variability within individual nights is based on the integral fluxes above 1 TeV and uses all data with zenith angles up to 45°.

In the following, only statistical errors will be discussed. The systematic uncertainty in relative flux values is esti-

mated to be smaller than 5%. Since the uncertainties in absolute fluxes are rather large, i.e., 30%, owing to the 15% uncertainty in absolute energy scale, we will quote not only absolute flux values but also the flux strength compared to that from the Crab Nebula. The HEGRA measurement of the integral flux above 1 TeV from the Crab Nebula is 16.7×10^{-12} photons cm^{-2} s^{-1} (Aharonian et al. 2000). The systematic uncertainty on the 500 GeV–5 TeV photon index is estimated to be 0.1.

3. RESULTS

3.1. *Light Curves*

The TeV gamma-ray and X-ray light curves as well as the 3–20 keV photon indices are shown as a function of time in Figures 1 and 2 for the 2000 February and May observations, respectively. The upper panels show the integral photon flux above 1 TeV, determined on a diurnal basis (*filled circles*). The results from observations with zenith angles below and above 30° are shown separately to take advantage of the higher sensitivity of the Cerenkov telescope system at zenith angles below $\sim 30°$. The diurnal mean integral fluxes vary from values compatible with zero to 25×10^{-12} photons cm^{-2} s^{-1} (1.5 times the integral flux of the Crab Nebula above 1 TeV). Bad weather conditions resulted in only 2 days with good TeV data during the May *RXTE* observation campaign.

The center panels of Figures 1 and 2 show the 3–20 keV X-ray flux. During the February and May observations, values of between 1.27×10^{-10} and 1.02×10^{-9} ergs cm^{-2} s^{-1} were observed. The TeV gamma-ray and X-ray fluxes are correlated in the sense that both fluxes show their maximum emission strength around MJD 51,581 (February 7) and 51,586 (February 12) and a minimum around MJD 51,584 (February 10). Note that the HEGRA observations have a mean duration of 1.8 hr, considerably longer than the mean duration of 18 minutes of the *RXTE* observations. Furthermore, not all HEGRA and *RXTE* observations had an overlap in time. As discussed in § 3.2, the TeV gamma-ray fluxes vary substantially on timescales as short as a fraction of an hour. A more detailed TeV gamma-ray/X-ray flux correlation analysis is hampered by the large statistical errors of the TeV flux estimates for adequately short integration times. This is shown by the open symbols in the upper panels of Figures 1 and 2. Here the HEGRA flux estimates have been computed with time bins of 15 minute durations, and only bins that overlap with *RXTE* observations are shown. Using 15 minute time bins, the statistical errors on the TeV flux estimates are comparable to the amplitude of the flux variability.

The lower panels in Figures 1 and 2 show the 3–20 keV photon indices. The photon indices vary from 2.9 for the days with the lowest flux level (MJD 51,587–51,590) to 2.2 for the days with the highest flux level (MJD 51,581, 51,667). The integral TeV gamma-ray fluxes and the results of the power-law fits to the X-ray data are summarized in Tables 1 and 2. For five observations with good photon statistics, the power-law fits do not describe the X-ray data satisfactorily; broken power-law fits will be discussed below.

3.2. *Shortest Variability Timescales*

We performed a search for the shortest TeV flux variability timescale based on a χ^2 analysis of the integral fluxes above 1 TeV determined with a 15 minute binning. The search revealed one night with significant flux variability. The integral fluxes above 1 TeV observed between MJD 51,582.06 and 51,582.27 (February 8) are shown in the

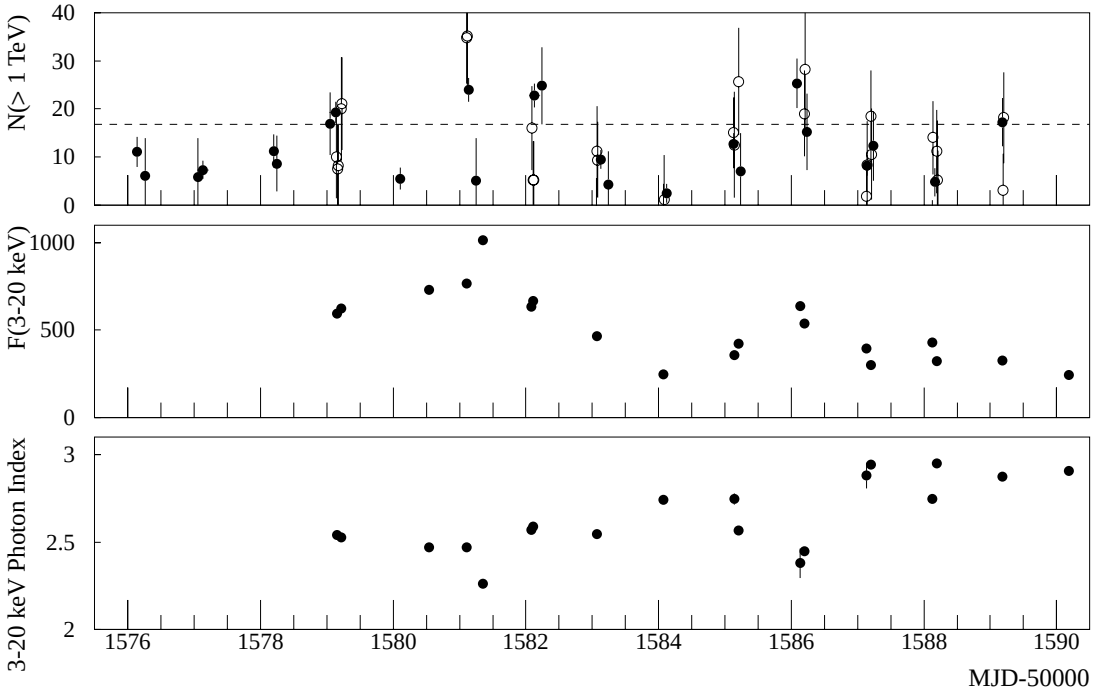

FIG. 1.—TeV gamma-ray and X-ray results from 2000 February. *Upper panel*: Integral flux above 1 TeV [$N(>1$ TeV)] in units of 10^{-12} photons cm^{-2} s^{-1}. Filled circles show the diurnal results separately for data from zenith angles below and above 30°; open circles show the flux as determined with 15 minute bins for all bins that overlap with *RXTE* observations. Dashed line indicates the steady flux level of the Crab Nebula. *Center panel*: 3–20 keV X-ray flux F(3–20 keV) in units of 10^{-12} ergs cm^{-2} s^{-1}. *Lower panel*: 3–20 keV photon index. MJD 51,576 corresponds to 2000 February 2.

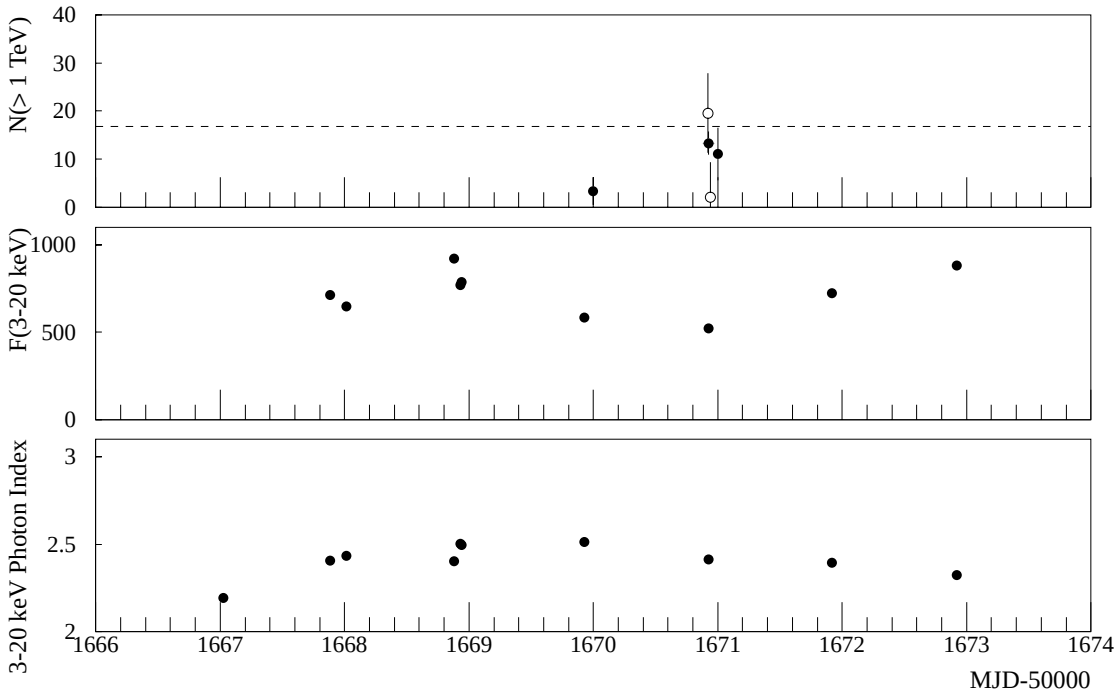

FIG. 2.—TeV gamma-ray and X-ray results from 2000 May. Symbols and units are the same as in Fig. 1. MJD 51,667 corresponds to 2000 May 3.

TABLE 1

INTEGRAL TeV FLUXES ABOVE 1 TeV

Start MJD	t_{obs}[a] (hr)	$N(>1$ TeV)[b] (10^{-12} photons cm^{-2} s^{-1})
51,576.1020.....	1.92	11.02 ± 3.12
51,576.2404.....	0.98	6.08 ± 7.87
51,577.0476.....	4.02	7.34 ± 1.91
51,577.0433.....	0.79	5.89 ± 8.05
51,578.1634.....	1.61	11.24 ± 3.41
51,578.2354.....	0.67	8.64 ± 5.76
51,579.0422.....	4.16	19.29 ± 2.18
51,579.0067.....	1.89	16.90 ± 6.52
51,580.0390.....	3.21	5.50 ± 2.28
51,581.0702.....	3.40	23.96 ± 2.49
51,581.2272.....	1.16	5.12 ± 8.86
51,582.0603.....	3.63	22.79 ± 2.43
51,582.2240.....	1.16	24.81 ± 7.99
51,583.0502.....	3.77	9.50 ± 2.00
51,583.2213.....	1.17	4.34 ± 6.83
51,584.0460.....	3.43	2.43 ± 1.93
51,585.0683.....	3.27	12.70 ± 2.22
51,585.2158.....	1.17	6.98 ± 7.93
51,586.0680.....	0.93	25.32 ± 5.19
51,586.2136.....	1.16	15.21 ± 7.96
51,587.0840.....	2.72	8.22 ± 2.17
51,587.2103.....	1.19	12.31 ± 7.25
51,588.1250.....	1.85	4.75 ± 2.91
51,589.1660.....	0.87	17.20 ± 5.02
51,669.9837.....	0.63	3.41 ± 2.87
51,670.8837.....	2.14	13.33 ± 2.42
51,670.9810.....	1.02	11.03 ± 5.47

NOTE.—Statistical errors only; see text for systematic errors.

[a] Net exposure.

[b] Integral flux above 1 TeV.

upper panel of Figure 3. Within 1 hr the TeV flux increases from a level consistent with zero to $(64 \pm 12_{stat}) \times 10^{-12}$ photons cm^{-2} s^{-1} ($3.9 \pm 0.7_{stat}$ crab). A fit of a constant to the integral fluxes is rejected with a chance probability of

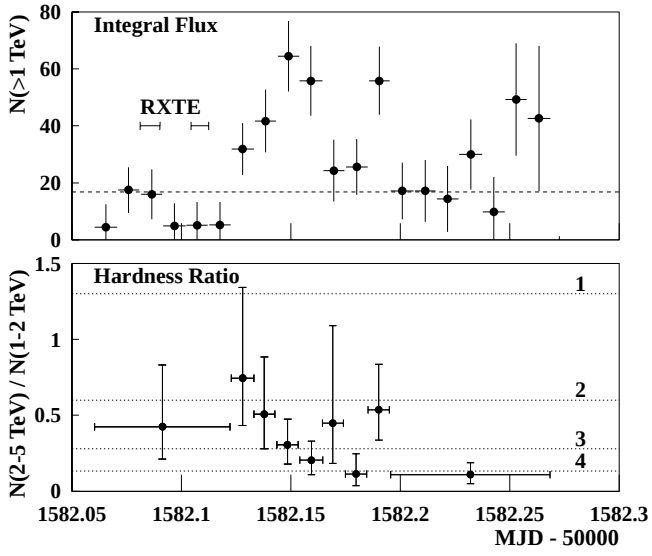

FIG. 3.—TeV gamma-ray results from 2000 February 8. *Upper panel*: Integral flux above 1 TeV [$N(>1$ TeV)] in units of 10^{-12} photons cm^{-2} s^{-1} with 15 minute bins. Dashed line indicates the steady flux level of the Crab Nebula; the two horizontal lines show the *RXTE* coverage. *Lower panel*: N(2–5 TeV)/N(1–2 TeV) hardness ratios (median values with 1 σ confidence intervals). Dotted lines show the expected hardness ratios for photon indices of 1, 2, 3, and 4, as labeled. Statistical errors only; see text for systematic errors.

TABLE 2

RESULTS OF POWER-LAW FITS TO THE 3–20 keV DATA

Start MJD	t_{obs}[a] (min)	$F_{3-20\ keV}$[b] (10^{-12} ergs cm^{-2} s^{-1})	Γ[c]	χ^2_r/dof[d]	P_c[e]
51,579.1485.....	18.1	385.3 ± 2.1	2.544 ± 0.012	1.22/38	0.17
51,579.2158.....	11.7	407.0 ± 2.6	2.527 ± 0.014	1.46/38	0.033
51,580.5430.....	52.5	496.9 ± 1.4	2.470 ± 0.006	3.10/38	4.1×10^{-10}
51,581.1048.....	14.4	521.5 ± 3.8	2.469 ± 0.016	1.17/38	0.21
51,581.3558.....	13.6	801.9 ± 4.8	2.262 ± 0.012	1.31/38	0.097
51,582.0812.....	13.1	402.7 ± 2.0	2.571 ± 0.011	1.18/38	0.2
51,582.1044.....	11.7	419.0 ± 2.2	2.588 ± 0.011	1.48/38	0.029
51,583.0693.....	24.0	300.2 ± 1.7	2.545 ± 0.012	1.34/38	0.077
51,584.0736.....	13.3	140.9 ± 1.7	2.743 ± 0.027	0.84/38	0.75
51,585.1369.....	4.0	203.5 ± 2.9	2.746 ± 0.031	0.71/38	0.91
51,585.2035.....	14.7	267.9 ± 1.7	2.568 ± 0.013	0.92/38	0.61
51,586.1333.....	0.3	460.1 ± 18.8	2.380 ± 0.085	0.78/38	0.84
51,586.2021.....	5.3	369.4 ± 3.8	2.450 ± 0.022	0.83/38	0.76
51,587.1320.....	0.8	207.9 ± 6.3	2.881 ± 0.072	0.77/38	0.84
51,587.2017.....	12.3	154.2 ± 1.7	2.942 ± 0.027	0.58/38	0.98
51,588.1279.....	12.8	245.4 ± 2.0	2.748 ± 0.019	0.89/38	0.67
51,588.1931.....	21.3	164.8 ± 1.3	2.950 ± 0.019	1.08/38	0.34
51,589.1891.....	22.1	172.2 ± 1.4	2.875 ± 0.018	1.16/38	0.23
51,590.1867.....	21.9	126.7 ± 1.2	2.909 ± 0.023	1.16/38	0.23
51,667.0272.....	24.0	1018.0 ± 1.8	2.195 ± 0.004	4.64/38	9.9×10^{-20}
51,667.8838.....	22.4	506.8 ± 2.1	2.405 ± 0.009	1.16/38	0.23
51,668.0120.....	18.1	451.8 ± 2.2	2.435 ± 0.010	0.79/38	0.81
51,668.8814.....	24.0	656.7 ± 2.2	2.401 ± 0.007	1.08/38	0.34
51,668.9321.....	7.2	511.1 ± 3.6	2.502 ± 0.015	0.89/38	0.67
51,668.9406.....	24.8	525.2 ± 2.0	2.495 ± 0.008	1.17/38	0.22
51,669.9278.....	49.6	385.1 ± 1.2	2.513 ± 0.007	1.55/38	0.016
51,670.9250.....	29.1	368.8 ± 1.1	2.412 ± 0.006	1.72/38	0.004
51,671.9206.....	28.5	517.1 ± 1.9	2.396 ± 0.008	2.06/38	1.4×10^{-4}
51,672.9231.....	11.5	664.6 ± 2.7	2.323 ± 0.008	1.65/38	0.007

NOTE.—Statistical errors only.

[a] Net exposure.

[b] The 3–20 keV flux.

[c] The 3–20 keV photon index.

[d] Reduced χ^2 value and dof of the power-law fit.

[e] Chance probability for larger reduced χ^2 values.

1.0×10^{-5}. Our observation of substantial TeV gamma-ray flux variability on subhour timescales confirms the existence of substantial subhour flux variations reported for the strong 1996 May 7 Mrk 421 flare (Gaidos et al. 1996).

The (2–5 TeV)/(1–2 TeV) hardness ratios are shown in the lower panel of Figure 3. The hardness ratios have been computed with the 1–2 and 2–5 TeV photon fluxes after correction for the (modest) zenith angle–dependent variation of the effective area over the considered energy range (Aharonian et al. 1999a). For a TeV energy spectrum of photon index Γ, the expected hardness ratio is then given by $r_{exp}(\Gamma) = (2^{-\Gamma+1} - 5^{-\Gamma+1})/(1 - 2^{-\Gamma+1})$ for $\Gamma > 1$ and $\ln(5/2)/\ln 2$ for $\Gamma = 1$. The values for $\Gamma = 1$, 2, 3, and 4 are shown as lines in the lower panel of Figure 3. The hardness ratios do not show evidence for spectral variability during the flare. A fit of a constant with a mean value of 0.23 gives a χ^2 value of 11.7 for 8 degrees of freedom (dof) corresponding to a probability of 16.5% for a higher value by chance. The data following MJD 51,582.225 has been taken under zenith angles larger than 30°, where systematic errors start to be nonnegligible. For these points (which do not enter strongly the χ^2 value cited above), the 1–2 TeV flux is uncertain by about 50%; accordingly, the latest hardness ratio point has a systematic error comparable to the statistical one. Unfortunately, *RXTE* observations were performed only during the first 1.5 hr of the 4.8 hr of HEGRA observations (see Fig. 3, *upper panel*) and did not cover the time of the strong TeV gamma-ray flare.

We analyzed the X-ray flux variability timescale by computing the *e*-folding times from the flux changes between observations: $\tau = \Delta t/\Delta \ln F(3\text{–}20\ \text{keV})$, with Δt the time difference between two observations and $\Delta \ln F(3\text{–}20\ \text{keV})$, the difference of the logarithms of the 3–20 keV fluxes. The shortest *e*-folding times are given in Table 3. Flux increases and decreases with *e*-folding times down to $\simeq 5.8$ and $\simeq 4.1$ hr, respectively, have been found.

We searched for rapid spectral changes by analyzing the change of spectral indices between *RXTE* observations. The fastest spectral changes are listed in Table 4. The fastest spectral variability is characterized by changes in photon index of $\simeq 0.12\ \text{hr}^{-1}$. We found similarly rapid spectral hardening as softening: on MJD 51,585 (February 11) the spectrum hardened by 0.18 in 1.6 hr, and on MJD 51,588 (February 14) the spectrum softened by 0.2 in 1.6 hr.

3.3. *TeV Gamma-Ray and X-Ray Energy Spectra*

In the energy range from 500 GeV to 5 TeV, the time-averaged spectrum of the February observations (MJD 51,576–51,589) is well described by a pure power-law model: $dN/dE = N_0(E/1\ \text{TeV})^{-\Gamma}$ with $N_0 = 25 \pm 1_{stat}$

TABLE 3

e-FOLDING TIMES OF THE FASTEST 3–20 keV FLUX INCREASES AND DECREASES

MJD1[a]	MJD2[b]	Δt[c] (hr)	τ[d] (hr)
51,585.1369.....	51,585.2035	1.6	5.82 ± 0.32
51,586.1333.....	51,586.2021	1.7	-7.54 ± 1.45
51,587.1320.....	51,587.2017	1.7	-5.61 ± 0.61
51,588.1279.....	51,588.1931	1.6	-4.12 ± 0.12
51,668.8814.....	51,668.9321	1.0	-4.32 ± 0.14
51,668.8814.....	51,668.9406	1.4	-6.38 ± 0.14

[a] Start of first observation.
[b] Start of second observation.
[c] Time difference between observations.
[d] The *e*-folding time.

photons cm^{-2} s^{-1} TeV^{-1} and $\Gamma = 2.94 \pm 0.06_{\rm stat}$. The fit has a χ^2 value of 15.6 for 7 dof (chance probability 5%). In Table 5 we give the results of the power-law fits for individual days for which the accuracy in the determined photon index is better than 0.3. The photon indices lie between 2.70 and 3.02, but the deviation from the mean index of 2.94 is statistically not significant. The large χ^2 value of the spectrum of MJD 51,582.0603 stems from two underpopulated bins centered at energies of 700 GeV and 4.35 TeV and indicates spectral softening with increasing energy. A more detailed discussion of the curvature of the TeV energy spectra that takes the systematic uncertainties fully into account is outside the scope of this paper and will be given in an upcoming paper in which the full data set of the year 2000 will be included.

TABLE 4

FASTEST CHANGES OF 3–20 keV PHOTON INDEX

MJD1[a]	MJD2[b]	Δt[c] (hr)	$\Delta\Gamma/\Delta t$[d] (hr^{-1})
51,581.1048.....	51,581.3558	6.0	-0.034 ± 0.003
51,585.1369.....	51,585.2035	1.6	-0.11 ± 0.02
51,586.1333.....	51,587.2017	25.6	0.022 ± 0.003
51,588.1279.....	51,588.1931	1.6	0.12 ± 0.02
51,668.8814.....	51,668.9321	1.1	0.09 ± 0.02

[a] Start of first observation.
[b] Start of second observation.
[c] Time difference between observations.
[d] Change in spectral index per 1 hr; negative values denote spectral hardening.

As shown in Table 2, a pure power-law fit does not give an acceptable fit to the data (chance probability well below 1%) for five *RXTE* observations with good photon statistics. We find that broken power-law models describe the data of these five pointings satisfactorily, and the results of fits to the 3–25 keV data are given in Table 6. The estimated break energies lie in the range between 6.6 and 8 keV, and the difference between the low- and high-energy power-law photon indices are about 0.2. Owing to the limited energy coverage of our X-ray observations, we did not fit the data with more complex models incorporating continuous spectral curvature. We investigated whether the other *RXTE* data sets were consistent with a similar change in spectral index by fitting these data sets with a broken power-law model with a fixed break energy at 7.3 keV (the mean break energy found for the data sets of Table 6). Indeed, all fits suggest spectral steepening, and we find a median value of the change in spectral index of 0.16, very similar to the mean change in spectral index of 0.19 found for the data sets of Table 6.

4. DISCUSSION

During our observation campaign, the X-ray photon index varied between values of 2.2 and 2.9. Cooling of a power-law distribution of electrons changes the synchrotron spectral index by at most 0.5 (Kardashev 1962). Therefore the observations clearly show that either the spectral index of accelerated particles is variable or we observe the cooling of electrons near the high-energy cutoff of the particle acceleration process. The TeV gamma-ray/X-ray emission of Mrk 421 is commonly attributed to the SSC mechanism (for alternative models see Aharonian 2000 and references therein) in which a population of high-energy electrons emits synchrotron radiation at longer wavelengths and high-energy photons from inverse Compton (IC) processes of high-energy electrons with lower energy synchrotron photons at shorter wavelengths.

Our initial modeling of the X-ray/TeV gamma-ray data with the time-dependent SSC code described by Coppi (1992) already allows some interesting conclusions that we will detail in the following. We focus on modeling the observations taken on an individual day, i.e., MJD 51,581, where a large change in X-ray flux and spectrum was observed and the TeV spectrum has been determined with reasonable statistical accuracy. We adopt a spherical emission volume of radius $R = 2.7 \times 10^{15}$ cm, which satisfies the constraints from the observed flux variability $R \lesssim \delta_j c \Delta T_{\rm obs} = 2.7 \times 10^{15}$ cm for a jet Doppler factor[11] $\delta_j = 50$ and flux varia-

TABLE 5

RESULTS OF POWER-LAW FITS TO THE 500 GeV–5 TeV DATA

Start MJD	$t_{\rm obs}$[a] (hr)	N_0[b] (10^{-12} photons cm^{-2} s^{-1} TeV^{-1})	Γ[c]	χ^2_r/dof[d]	P_c[e]
51,579.0422.....	4.16	$33.51^{+2.76}_{-3.16}$	$2.76^{+0.16}_{-0.14}$	1.42/8	0.18
51,581.0702.....	3.40	$44.21^{+2.71}_{-3.37}$	$2.70^{+0.14}_{-0.10}$	0.54/8	0.83
51,582.0603.....	3.63	$36.27^{+2.99}_{-2.76}$	$2.72^{+0.12}_{-0.10}$	3.05/8	0.002
51,583.0502.....	3.77	$19.63^{+2.92}_{-3.20}$	$2.98^{+0.34}_{-0.24}$	0.87/8	0.54
51,585.0683.....	3.27	$24.90^{+3.14}_{-3.22}$	$3.02^{+0.28}_{-0.24}$	1.09/7	0.47

NOTE.— Statistical errors only; see text for systematic errors.
[a] Net exposure.
[b] Normalization constant.
[c] Power-law photon index.
[d] Reduced χ^2 value and dof.
[e] Chance probability for larger reduced χ^2 values.

TABLE 6

RESULTS OF BROKEN POWER-LAW FITS TO THE 3–25 keV DATA

Start MJD	t_{obs}[a] (min)	$k_{1\ keV}$[b] (photons keV^{-1} cm^{-2} s^{-1})	E_b (keV)	Γ_1[c]	Γ_2[d]	χ_r^2/dof[e]	P_c[f]
51,580.5430.....	52.5	$0.383^{+0.005}_{-0.006}$	$7.40^{+0.28}_{-0.32}$	$2.415^{+0.009}_{-0.010}$	$2.646^{+0.026}_{-0.027}$	1.11/46	0.281
51,667.0272.....	24.0	$0.456^{+0.005}_{-0.005}$	$6.96^{+0.31}_{-0.28}$	$2.137^{+0.007}_{-0.008}$	$2.301^{+0.014}_{-0.012}$	1.19/46	0.173
51,670.9250.....	29.1	$0.255^{+0.005}_{-0.005}$	$6.60^{+0.81}_{-0.49}$	$2.358^{+0.015}_{-0.014}$	$2.520^{+0.034}_{-0.023}$	0.67/46	0.957
51,671.9206.....	28.5	$0.353^{+0.007}_{-0.008}$	$8.03^{+1.07}_{-1.03}$	$2.357^{+0.013}_{-0.017}$	$2.560^{+0.069}_{-0.053}$	1.09/46	0.310
51,672.9231.....	11.5	$0.385^{+0.009}_{-0.009}$	$7.46^{+0.84}_{-0.55}$	$2.268^{+0.016}_{-0.015}$	$2.477^{+0.048}_{-0.035}$	0.75/46	0.897

NOTE.—Statistical errors only.
[a] Net exposure.
[b] Flux at 1 keV.
[c] Low-energy photon index.
[d] High-energy photon index.
[e] Reduced χ^2 value and dof.
[f] Chance probability for larger reduced χ^2 values.

bility timescale $\Delta T_{obs} = 30$ minutes. We assume a randomly oriented magnetic field of mean strength $\boldsymbol{B} = 0.22$ G (in jet frame). For this magnetic field, electrons of Lorentz factor $\gamma_e = 1.8 \times 10^5$ that produce synchrotron radiation with maximum power per logarithmic energy band at energy $\varepsilon \approx (3/4\pi)\delta_j he\langle \sin\theta \rangle$ keV (h is Planck's constant, e the electron charge, $\langle \sin\theta \rangle = (\frac{2}{3})^{1/2}$) have an observed radiative cooling time $t_s = [(4/3)\sigma_T c\delta_j(\boldsymbol{B}/8\pi m_e c^2)\gamma_e]^{-1}$ (σ_T is the Thomson cross section of ≈ 30 minutes, comparable to the fastest variability timescale during the observation campaign). We inject a power law of accelerated electrons $q(\gamma_e, t) = \text{const} \times \gamma_e^{-P} \exp[-\gamma_e/\gamma_{max}(t)]$ with $P = -2$ (the expected value for diffuse particle acceleration at strong shocks) and assume a Hubble constant of $H_0 = 60$ km s^{-1} Mpc^{-1} and a deceleration parameter of $q_0 = 0.5$.

Following Mastichiadis & Kirk (1997), we model the temporal evolution of X-ray flux and spectrum by changing γ_{max} only. We use a damping term for the electron density inside the source of $\partial n_e/\partial t \propto -n_e/t_{esc}$, with an escape time t_{esc} of 5 light-crossing times. We use a minimum Lorentz factor of accelerated particles of $\gamma_{min} = m_p/m_e = 1836$ (ratio of proton to electron mass), above which diffusive shock acceleration is probable to work (Eilek & Hughes 1991). The results in the X-ray and TeV energy ranges do not depend strongly on the value of γ_{min} (as long as it is smaller than $\approx 10^4$), and the model does not need fine-tuning of these parameters. Conversely, the emission strength in the infrared and optical bands do depend on the value of γ_{min}. A multiwavelength campaign with observations in these bands, together with X-ray and TeV gamma-ray coverage, would make it possible to assess this important parameter of particle acceleration theories.

The solid lines in Figure 4 show the results of calculations in which we modeled the relatively high flux level observed on MJD 51,581 by changing γ_{max} from an initial value of 1.4×10^5 to a maximum value of 5.0×10^5. The model satisfactorily describes the X-ray flux, the X-ray spectral index, and the TeV flux. Note that the observational coverage is much too sparse to pin down the temporal evolution of the source. Very different choices of the temporal evolution of the maximum Lorentz factor of accelerated particles $\gamma_{max}(t)$ are able to describe the data, as shown by, e.g., the dashed lines in Figure 4. Some properties of the SSC model calculations, however, do not depend strongly on the adopted hypothesis of what causes individual flares. In the following we will focus on these properties.

Figure 5 compares the observed SEDs with the ones from the SSC model (model 1, shown by solid lines in Fig. 4). Given the constraints on the size of the emission volume from the observed flux variability, we did not achieve a fit of the combined X-ray and TeV gamma-ray data with jet Doppler factors substantially below 50. Lower Doppler factors resulted either in a strong overproduction of TeV gamma rays for small values of the mean magnetic field ($\boldsymbol{B} \ll 0.22$ G) or in a too steep TeV energy spectrum for high values of the mean magnetic field ($\boldsymbol{B} \gg 0.22$ G). A sharper high-energy cutoff in the spectrum of accelerated particles also did not reduce the IC photon yield substantially. Reducing the jet Doppler factor by using a minimum

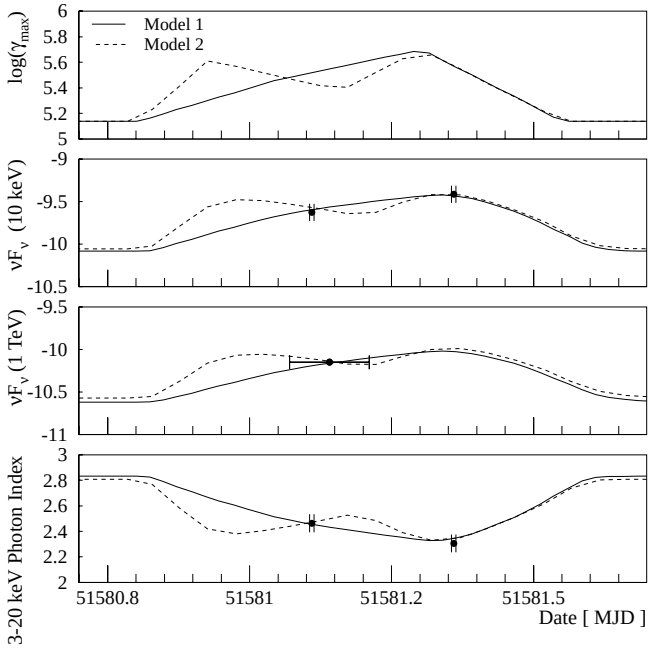

FIG. 4.—From above to below the cutoff electron Lorentz factor, the energy flux at 10 keV and 1 TeV and the 3–20 keV photon indices are shown for the data (*filled circles*; horizontal error bars show the length of the observations) and two models (*dashed and solid lines*). All energy fluxes are in units of 10^{-12} ergs cm^{-2} s^{-1}. See text for model parameters and systematic errors on the data points.

[11] The jet Doppler factor is defined as $\delta_j^{-1} = \Gamma(1 - \beta \cos\theta)$, with Γ the bulk Lorentz factor and β the bulk velocity in units of the speed of light and of the emitting volume, respectively, and θ is the angle between jet axis and the line of sight as measured in the observer frame.

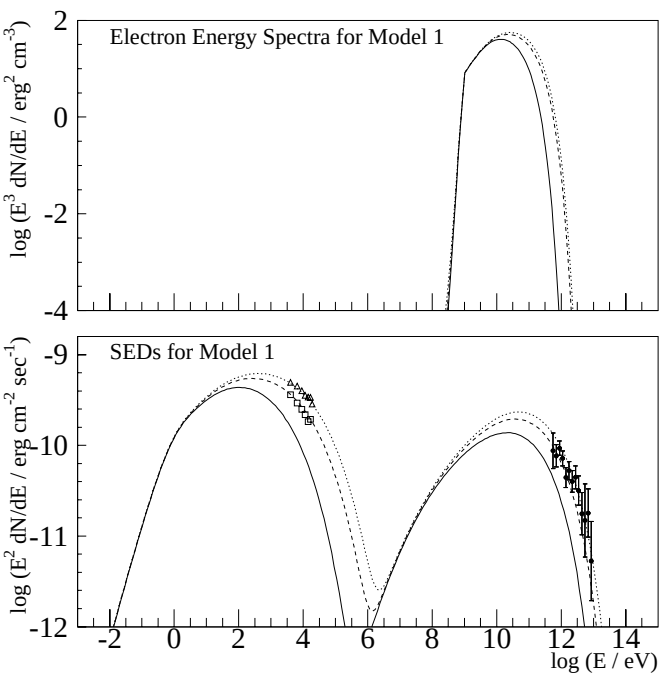

FIG. 5.—*Upper panel*: Model estimate for the electron density in the emission region (times the third power of energy); *lower panel*: observed (*symbols*) and modeled (*lines*) SEDs. Electron energies are given in the jet frame and the photon energies in the observer frame. Model estimates correspond to the solid lines of Fig. 4. Squares and the triangles show the *RXTE* spectra measured from 51,581.1048–51,581.1148 and 51,581.3557–51,581.3652, respectively. Filled circles show the HEGRA data measured during MJD 51,581.0702–51,581.2119, which included the first *RXTE* pointing (statistical errors only, see text for systematic errors). Solid, dashed, and dotted lines show the model of the low-flux spectrum before the flare and during the first and second *RXTE* pointings, respectively. Note that the model prediction for the HEGRA spectrum is to very good approximation shown by the dashed line.

Lorentz factor of accelerated particles requires $\gamma_{\rm min}$ values of several times 10^4, which is difficult to motivate theoretically. Taking into account extragalactic extinction would result in even higher Doppler factors since the effect is expected to substantially steepen the observed TeV gamma-ray spectrum while reducing the gamma-ray flux around 1 TeV by a factor $\lesssim 2$ (Stecker & De Jager 1998; Primack et al. 2001). Furthermore, external seed photons, neglected in our analysis, would result in an even higher model prediction of the emitted TeV gamma-ray flux.

Our modeling differs from earlier work that indicated Doppler factors of about 15 (see, e.g., Inoue & Takahara 1996; Mastichiadis & Kirk 1997; Takahashi et al. 2000) because of one or several of the following reasons: we use a small emission volume (consistent with flux variability on a 30 minute timescale); we use a minimum Lorentz factor of accelerated electrons well below 10^4; and we use snapshots of an evolving electron spectrum instead of steady state electron spectra. Since the cooling times of the electrons responsible for the X-ray and TeV gamma-ray emission are comparable to the duration of individual flares, steady state electron populations overestimate the extent to which electron spectra cool before, during, and after individual flares. Note that SSC models with Doppler factors of about 15 predict, in agreement with the results of our code, TeV energy spectra softer than the ones that have been observed so far (Inoue & Takahara 1996; Takahashi et al. 2000).

For high Doppler factors, the energy density of relativistic electrons and of the magnetic field are more comparable than for low Doppler factors (compare Inoue & Takahara 1996): for our choice of $\gamma_{\rm min}$ and δ_j the energy density of relativistic particles is $u_e \approx 0.01$ ergs cm^{-3} and that of the magnetic field is $u_{\boldsymbol{B}} \approx 0.002$ ergs cm^{-3}. The model requires a modest minimum kinetic power (see, e.g., Begelman, Rees, & Sikora 1994) transported by the jet $L_j = \Gamma^2(u_e + u_p + u_{\boldsymbol{B}})cr^2\Delta\Omega$ of $\approx 4.25 \times 10^{43}$ ergs s^{-1}. Here we assumed $\Gamma = 50$, a distance of the emission region from the central engine of $r = 10^{16}$ cm, and a solid angle subtended by the jet of $\Delta\Omega \approx 2\pi[1 - \cos(\Gamma^{-1})] = 1.26 \times 10^{-3}$ sr. Furthermore we assumed a factor of $\kappa = 1000$ more cold electrons than relativistic electrons (the density of relativistic electrons in our models is ≈ 3 cm^{-3}) and an equal number of electrons and cold protons, giving a comoving energy density in cold protons of $u_p = 4.5 \times [(\kappa + 1)/1001]$ ergs cm^{-3}.

In accordance with earlier observations (Gaidos et al. 1996; Takahashi et al. 1996; Maraschi et al. 1999; Fossati et al. 2000a), we find shorter flux variability at TeV energies than at X-ray energies with shortest *e*-folding times of ≈ 1 hr at TeV energies and ≈ 5 hr at X-ray energies, respectively. This finding could naturally be explained in the framework of an inhomogeneous SSC model. If the region of particle acceleration is relatively small, an event of enhanced particle acceleration could result in a rapidly variable TeV gamma-ray component originating from the vicinity of the acceleration region while the observed X-rays, dominated by the emission of particles of earlier acceleration events, could vary more slowly. If strong internal shocks accelerate the electrons, one indeed expects that the accelerated particles are bound to the downstream medium by the same scattering processes that enable particle acceleration. If the density of relativistic particles decreases downstream (because of particle diffusion or adiabatic expansion of the downstream plasma), the SSC mechanism then guarantees that the IC emissivity decreases faster than the synchrotron emissivity. Although the synchrotron emission of such a system has been discussed in the literature (see, e.g., Heavens & Meisenheimer 1987; Kirk, Rieger, & Mastichiadis 1998), the consequences for the temporal evolution and correlation of the synchrotron and the IC components have not yet been studied. The upcoming Cerenkov telescope experiments CANGAROO III, HESS, MAGIC, and VERITAS with 1 order of magnitude higher sensitivity than present instruments will make it possible to test such inhomogeneous models and to infer details about the geometry and dynamics of the radiating plasma. To "map" in this way the jet at its base in the very vicinity of the black hole is a very exciting prospect of gamma-ray astronomy indeed.

We thank Jean Swank and the *RXTE* GOF for allowing us to use the *RXTE* time for Mrk 421 observations. The support of the German Ministry for Research and Technology BMBF and of the Spanish Research Council CYCIT is gratefully acknowledged. We thank the Instituto de Astrophysica de Canarias for the use of the site and for supplying excellent working conditions at La Palma. We gratefully acknowledge the technical support staff of the Heidelberg, Kiel, Munich, and Yerevan institutes. Rita Sambruna is supported by NASA AOP grant NAG 5-27016.

REFERENCES

Aharonian, F. A. 2000, NewA, 5, 377
Aharonian, F. A., et al. 1999a, A&A, 342, 69
———. 1999b, A&A, 349, 11
———. 1999c, A&A, 350, 757
———. 2000, ApJ, 539, 317
Begelman, M. C., Rees, M. J., & Sikora, M. 1994, ApJ, 429, L57
Buckley, J. H., et al. 1996, ApJ, 472, L9
Coppi, P. S. 1992, MNRAS, 258, 657
Dickey, J. M., & Lockman, F. J. 1990, ARA&A, 28, 215
Eilek, J. A., & Hughes, P. A. 1991, Beams and Jets in Astrophysics, ed P. A. Hughes (Cambridge: Cambridge Univ. Press)
Fossati, G., et al. 2000a, ApJ, 541, 153
———. 2000b, ApJ, 541, 166
Gaidos, J. A., et al. 1996, Nature, 383, 319
Gorham, P. W., van Zee, L., Unwin, S. C., & Jacobs, C. 2000, AJ, 119, 1677
Guainizzi, M., Vacanti, G., O'Flaherty, K. S., Palazzi, E., & Parmar, A. N. 1999, A&A, 342, 124
Heavens, A. F., & Meisenheimer, K. 1987, MNRAS, 225, 335
Inoue, S., & Takahara, F. 1996, ApJ, 463, 555
Jahoda, K., et al. 1996, Proc. SPIE, 2808, 59
Kardashev, N. S. 1962, Soviet Astron., 6(3), 317
Kirk, J. G., Rieger, F. M., & Mastichiadis, A. 1998, A&A, 333, 452
Konopelko, A., et al. 1999, Astropart. Phys., 10, 275
Krennrich, F., et al. 1999, ApJ, 511, 149
Malizzia, A., et al. 2000, MNRAS, 312, 123
Maraschi, L., et al. 1999, Astropart. Phys., 11, 189
Mastichiadis, A., & Kirk, J. G. 1997, A&A, 320, 19
Petry, D., et al. 1996, A&A, 311, L13
Primack, J. R., Somerville R. S., Bullock J. S., & Devriendt, J. E. G. 2000, in AIP Conf. Proc. 558, High-Energy Gamma-Ray Astronomy, ed. F. Aharonian & H. Völk (New York: AIP, 463)
Punch, M., et al. 1992, Nature, 358, 477
Rothschild, et al. 1998, ApJ, 496, 538
Schubnell, M. S. 1996, A&AS, 189, 3105
Stecker, F. W., & De Jager, O. C. 1998, A&A, 334, L85
Takahashi, T., et al. 1996, ApJ, 470, L89
———. 2000, ApJ, 542, L105